# Quantitative Fracture Surface Analysis

Terry A. Michalske, Sandia National Laboratories

FRACTURE SURFACE MARKINGS (FSM) can be used to draw quantitative conclusions about a fracture event because a passing fracture front leaves a permanent record of its history in the form of topographic markings (Ref 1–3). The FSM can be used to locate the failure origin and determine how the catastrophic crack developed under the influence of the applied and transient stress fields. The FSM also show how the microstructure and processing defects in the material influenced the catastrophic failure event.

The clues left behind by FSM are used to investigate the circumstances surrounding a failure event (during service life or testing) in hopes of answering questions such as:

- What was the nature of the defect that originated failure?
- What was the magnitude of the applied stress at failure?
- What was the stress state at failure (uniaxial tension, biaxial tension, and so forth)?
- Did factors such as residual stresses or the presence of stress-corrosion environments influence the failure event?

Quantitative answers to these questions are obtained by employing a combination of fracture mechanics-based and empirically based relations to convert measurements obtained from FSM to quantitative estimates for the pertinent fracture parameters. Fracture surface markings also are used to develop realistic models for failure mechanisms in a new material.

## Fracture Features

This article discusses how important fracture features are developed, measured, and converted into a quantitative measure of the fracture conditions. For simplicity, the principle of quantitative fracture surface analysis will concentrate on isotropic, homogeneous brittle materials (for example, glasses) and then show how anisotropic crystalline or polycrystalline properties of a ceramic material may influence the characteristics of the FSM.

The basic feature of all failures begins at a specific point called the failure origin. Once the failure origin has been identified, the origin flaw size can be used to estimate the magnitude of the stress at failure. As the fracture spreads away from the failure origin, the fracture velocity may increase. The formation of FSM such as mist, hackle, and branching, which indicate high-velocity fracture, can also be used to estimate the magnitude of stress at failure. Wallner lines offer a "shapshot" of the crack front as it passes through the material. The spacing between and the intersection of Wallner lines that are created during the fracture process can provide a quantitative, local measure of the stresses in the material. The fragmentation pattern created by the branching of the primary crack provides information about the magnitude and state of the applied stress (uniaxial or biaxial tension). Finally, effects such as residual stress and stress-corrosion cracking can be quantitatively assessed through measurements on the fracture surface. Each of these features are described in subsequent sections of this article.

**Fracture Mechanics Relations.** As indicated in the introduction, some of the quantitative aspects of fracture surface analysis are based upon continuum elastic fracture mechanics relations. The following discussions provide a brief description of the fracture mechanics relations that are used in quantitative fractographic analysis. Other articles in the Section "Failure Analysis" of this Volume provide more detailed discussions on the application of fracture mechanics to the failure of ceramic materials.

The most fundamental of fracture mechanics parameters is the crack tip stress intensity ($K_I$). When a continuous elastic material containing a crack is exposed to an externally applied stress, a concentrated field of stress is developed near the tip of a crack or flaw in the material. This stress field, which is concentrated by the crack in the material, produces the locally high stresses that lead to material failure and crack propagation. The magnitude of the stress field local to the crack tip is described by the $K_I$ parameter. Fracture mechanics formulations show that the magnitude of $K_I$ is given by:

$$K_I = \sigma Y \sqrt{a} \qquad \text{(Eq 1)}$$

where $\sigma$ is the applied stress, $a$ is the leng of the crack, and $Y$ is a parameter that accou for the crack geometry. Equation 1 h important applications in failure analysis glass and ceramic materials. If we can dete mine the size and shape of a crack and t magnitude of the external stress, we c identify a unique value of the crack tip stre intensity that will cause crack propagation the material of interest. In practice, we u one of a number of controlled geometry fra ture mechanics tests (Ref 4) to measure t value of $K_I$ for crack propagation. The stre intensity value for catastrophic propagation referred to as the critical stress intensity ($K_{Ic}$ The critical stress intensity is an extreme useful parameter in brittle materials failur since it provides a single parameter to describ the resistance of the material to crack pro agation. In fact, Eq 1 can be rewritten as:

$$\sigma_f = \frac{K_{Ic}}{Y\sqrt{a}} \qquad \text{(Eq 2}$$

where $\sigma_f$ is the failure strength. Using thi relation and the measured value for $K_{Ic}$, on can predict a practical strength for the cerami material as a function of flaw size.

The fracture mechanics approach to mate rials strength allows us to understand an predict the effect of surface flaws on th strength of glasses and ceramic materials. W can easily see from Eq 2 that increasing th size of the surface flaws will greatly decreas the materials strength.

This limited discussion treats fracture as an on-off process. At applied stress intensities below $K_{Ic}$, no crack propagation occurs whil above $K_{Ic}$, the material catastrophically frac tures. In many engineering materials of inter est, once a crack begins to propagate, the spee of the advancing crack will be dependent upon the magnitude of $K_I$. Because the crack speed increases very rapidly with increasing $K_I$, the magnitude of the error introduced by considering fracture as an on-off process is usually quite small. Only in special cases, particularly in the presence of chemically reactive environments, does this on-off approximation of the fracture event produce significant errors. In the section "Stress-Corrosion Frac-

ture" of this article, the topic of stress corrosion in glass and ceramics and the fracture surface markings associated with that regime of failure is explored.

## Origin Flaw

As its name implies, the origin flaw is the defect from which the entire fracture event develops. For this reason it is one of the most important features imprinted on the fracture surface. Location of the origin flaw is determined by the fractographic methods described in the article "Descriptive Fractography" in this Volume. Once the origin flaw is located, then its size can be used to quantitatively estimate the magnitude of stress at failure and to quantitatively interpret the event that produced the failure origin.

Failure origins are any topographic or compositional features that concentrate the applied stress to a magnitude that locally exceeds the fracture strength of the material. These features can be processing related as in the case of pores or inclusions, or they may be small surface cracks. In brittle ceramic or glassy materials, surface cracks are often generated by mechanical contact or surface abrasion events. In these hard materials, mechanical contact usually occurs at surface asperities. Localized contact generates large elastic stresses that are confined to the area of contact. When the local stress exceeds the materials strength, a surface flaw is created which develops only in the region of locally high stress. The resultant surface crack concentrates the applied stress (as previously discussed in the section "Fracture Mechanics Relations") and can serve to nucleate the catastrophic fracture event.

**Identification and measurement of origin flaw size** is possible because its boundary will be outlined by an arrest line. The arrest line that indicates the origin flaw is often easy to detect since the localized stress field that produced the origin flaw will not be oriented in exactly the same way as the applied stress that causes failure. Because cracks always propagate normal to the applied stress field, the plane of the origin flaw will be inclined with respect to the plane of catastrophic crack propagation and can easily be observed in reflected light conditions (Fig 1).

**Estimating Failure Stress from Origin Flaw Size.** After the size of the cracking origin is determined, linear elastic fracture mechanics (Eq 2) can be used to evaluate the applied stress that would have caused failure. Values for $K_{Ic}$ are available for most glass and ceramic materials and can be obtained from materials properties handbooks (Ref 5, 6). The geometric factor ($Y$) for various idealized flaw shapes is available in linear elastic fracture mechanics complications (Ref 7). In the case of a well-defined surface crack, one should be able to use the technique described above to convert a measured crack size on the fracture surface into an estimate for the failure stress.

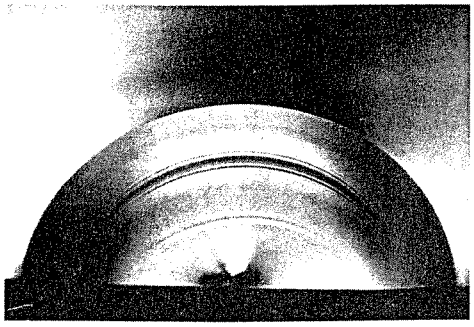

**Fig 1** Semicircular fracture origin in glass surface. Slight differences in orientation of the origin flaw allow it to be distinguished from subsequent fracture plane using reflected light microscopy. 25×

However, extreme caution should be used when applying the above method for estimating the stress at failure. Many of the surface flaws encountered in practice are far from idealized geometries (see Fig 2), and it may be difficult to determine an appropriate $Y$ value to account for their stress-concentrating effect. For the case of well-defined flaws, the errors associated with the geometric factor are not large (less than a factor of 30%, Ref 8) and should not prevent a reasonable estimate of the failure stress. A more serious problem is that the origin flaw will most likely not be aligned with the direction of the applied stress that precipitates catastrophic failure. The relation given in Eq 2 only holds true for origin cracks that are aligned with the applied stress at failure. As the alignment between the origin flaw and the applied stress becomes worse, the stress-concentrating power of a given size crack will decrease and cause one to severely underestimate the failure stress.

When the flaw size is used to estimate the failure stress in polycrystalline materials, the above-mentioned precautions must be observed as well as a consideration for the effect of the microstructure. Mecholsky *et al.* (Ref 8) has reviewed the effect of microstructure on flaw size estimates of failure stresses. They show that errors in failure stress determinations can be attributed to two separate effects: a microstructure dependent value for $K_{Ic}$ and the generation of local residual stresses. Several studies have shown that the inherent fracture resistance of a material is affected by the ratio of the flaw size to the grain size (Ref 9, 10). In most cases, $K_{Ic}$ increases as the flaw size/grain size increases. This effect would cause one to overestimate the failure strength that was determined from measurements of a small flaw, because values for $K_{Ic}$ are normally determined from large-crack fracture mechanics test techniques (Ref 4).

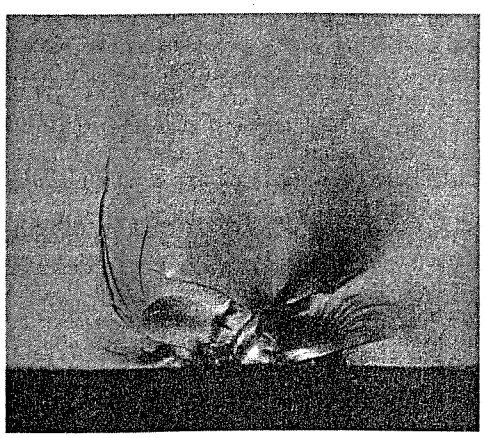

**Fig 2** Typical failure origin in glass produced by asperity contact at glass surface. In practice, the complex geometry of failure origins can make flaw size determinations difficult. Reflected light, 50×

Local residual stresses can arise from thermal expansion anisotropies in the grains of a polycrystalline material. In the case of flaws that are large with respect to the grain size, the flaw will span several grains and the effect of the local stresses are expected to average out. However, a flaw that encompasses only one or two grains may be subject to a large residual stress contribution. This stress contribution may either add or subtract from the applied stress and therefore can cause an under- or overestimate in the failure stress.

In the case of noncracklike origin flaws such as pores or inclusions, it is not generally possible to evaluate the magnitude of the applied stress from measurements of the defect size. In the case of a spherical pore the stress concentration is independent of the size of the pore (Ref 11). Therefore, the size of the pore alone cannot be used to estimate the failure stress during an investigation after failure. The stress concentration around an inclusion of a foreign material is extremely difficult to evaluate because it depends not only on the shape of the inclusion but also on the thermal expansion and elastic mismatch between the inclusion and the matrix, and on the strength of the interfacial bond between the inclusion and the matrix. All of these factors contribute to the stress concentration in a defect and make it extremely difficult to use the inclusion size to estimate failure stress.

**Geometric Characteristics of Surface Cracks Caused by Contact Stresses.** In the preceding section, the size of an origin flaw is used to estimate the failure stress. In the case of surface cracks caused by localized contact stresses, some quantitative aspects of the contact event can be determined from the size of a crack origin. Hertz (Ref 12), for example, studied the elastic problem of a sphere contacting a flat surface and showed that the largest tensile stresses occur at the flat surface just outside the radius of mutual contact. This stress distribution produces a cone crack that initiates just outside the zone of mutual contact (Fig 3). Lawn *et al.* (Ref 13) have shown that the size of the cone crack ($R$) can be related to the normal load ($P$) as follows:

$$P^2/R^3 = Eb \qquad \text{(Eq 3)}$$

where $E$ is the elastic modulus of the sub-

strate, and $b$ is an empirically derived constant that must be evaluated for the material of interest. By measuring the diameter and depth of the Hertzian cone flaw, one can estimate the size and normal force of the projectile that contacted the surface.

For the case of highly angular contact asperities, fracture mechanics formulations for pyramidal indenters can be used to guide the quantitative fractographic analysis. Figure 4 shows the surface flaw geometry developed by contact with an angular asperity. Marshall *et al.* (Ref 14) examined the cracking around indenter tips and have shown that crack size can be related to the indenter force as follows:

$$P = \frac{(\sqrt{a})^3 K_{Ic}}{\chi} \qquad \text{(Eq 4)}$$

where $P$ is the indenter load, $a$ is the length of the radial cracks, and $\chi$ is an empirical parameter that must be determined for the specific material. Wiederhorn (Ref 15) has used this relation to examine erosion of glass and ceramic surfaces by angular particle impact. He has shown that the particle impact parameters can be estimated from inspection of the resulting surface cracks.

## Mirror Region of Crack Propagation

Once the catastrophic crack has been nucleated, it will begin to spread from the origin under the influences of the applied stress field. The early stage of crack propagation produces a region which is very smooth and flat and is often referred to as the mirror. In glass, which has no microstructural detail, this region appears mirror smooth. In materials with microstructural details, however, the roughness of the mirror region will be dictated by the scale of the microstructure.

**Wallner Lines.** Within the mirror region of crack propagation, transient variations in the stress field will result in undulations in the crack path that will appear as Wallner lines (Ref 16) on the fracture-generated surface. As previously indicated, a crack will always propagate normal to the applied tensile stress field. When a transient stress wave acts to tilt the local applied stress, the crack will respond

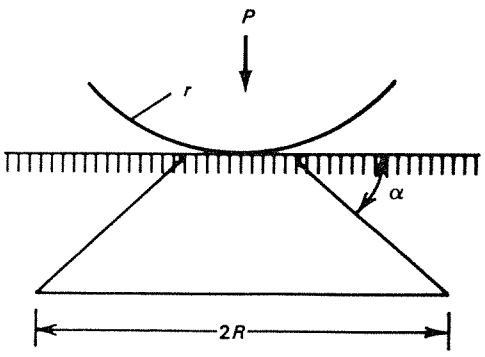


**Fig 3** Hertzian cone fracture pattern produced by spherical particle contact with flat surface

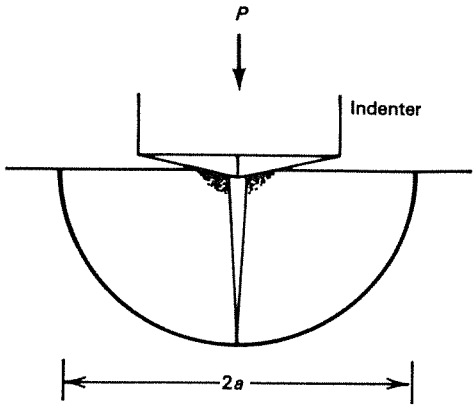


**Fig 4** Radial fracture pattern developed by pyramidal indenter contact with flat surface

to the changing stress field by altering its plane of propagation during the transient event. As a transient stress wave sweeps past the propagating crack, the Wallner line that is developed will represent a snapshot of the crack front shape and position during the transient event. The stress transients that produce Wallner lines can be the result of:

- A crack front passing an inclusion or pore in the material that alters the local stress field
- The mechanical ringing of the sample as stress waves reflect across the interior of the sample during failure

**Determination of Crack Velocity.** Poncelet (Ref 17) has shown that the intersection of Wallner lines formed by two separate transient stress events can be used to determine the velocity of the advancing crack front. Figure 5 shows the geometric identities that are involved in determining the crack velocity from Wallner line intersection. This analysis provides an important means of quantitatively determining the local crack velocity from measurements of the FSM.

Ultrasonic fractography can also be used to assess the local crack velocity. In this technique, Wallner lines are produced by purposefully inducing a pattern of transient stress pulses during crack propagation. A piezoelectric or other electrochemical device is used to generate a series of controlled period stress transients. These stress transients produce a series of Wallner lines with a known temperal distribution (Fig 6). One needs only to measure the spacing between these lines on the fracture surface and divide by the period of the stress pulse signal to accurately determine the local crack velocity. This approach to crack velocity measurement is often referred to as ultrasonic fractography. The original studies (Ref 18–20) utilizing this approach were designed to investigate high-speed fracture events (crack velocity > 100 m/s), and so the frequency of stress pulses was necessarily in the MHz range. However, more recent applications of this technique (Ref 21–23) have shown that it can be used to examine crack

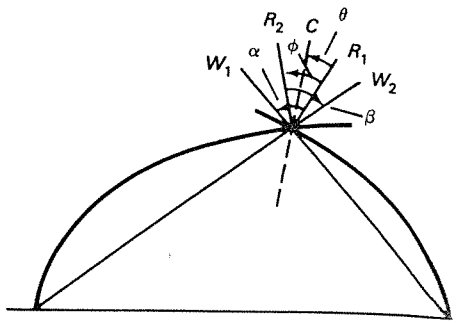


$$\frac{\text{Crack velocity}}{\text{Wave velocity}} = \frac{\sin\theta}{\sin\alpha}$$

$$\frac{\sin\theta}{\sin\alpha} = \frac{\sin\phi}{\sqrt{(\sin^2\phi\sin^2\alpha + (\cos\phi\sin\alpha - \sin\beta)^2}}$$

$$\tan\theta = \frac{\sin\phi}{\cos\phi - \sin\beta/\sin\alpha}$$

$$\sin\beta < 0$$

**Fig 5** Identities used to determine the crack velocity from the intersection of two Wallner lines on the fracture surface. $R_2$ and $R_1$ are lines drawn normal to each Wallner line at the point of intersection. C is a line drawn from the point of intersection to the failure origin.

velocities as low as $10^{-3}$ m/s (0.04 in./s) using low-frequency stress pulse signals.

Detailed information about the crack velocity can provide very much important information concerning the stress field responsible for the fracture event. Fracture mechanics studies have shown that a unique relation exists between the crack velocity ($V$) and the stress intensity ($K_I$). (The details of this relationship are discussed in the section "Stress-Corrosion Fracture" of this article.) By using the $K_I$ versus $V$ relationship and measuring the local crack velocity by fractographic techniques one can accurately measure the local stress intensity of a propagating crack. Michalske *et al.* (Ref 22–23) have used this approach to experimentally assess the

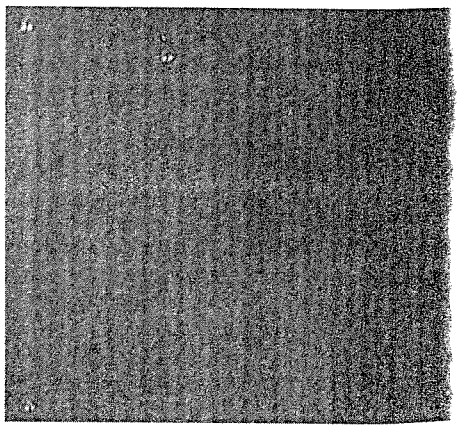

**Fig 6** Wallner lines produced by imposing a periodic stress onto the static stress applied during crack propagation. Differential interference contrast. 50×

validity of fracture mechanics test methods and fracture mechanics analysis of various surface flaw geometries.

## Mirror Radius

As a catastrophic crack continues to spread out from the origin under the influence of a constant applied stress, it may accelerate until it reaches its "terminal" velocity. Under static loading conditions, crack velocities in brittle materials have been observed by use of ultrasonic fractography and high-speed fractography to reach about six-tenths the Rayleigh wave speed (Ref 20). As the terminal velocity is approached, the fracture surfaces lose their mirror smooth condition and begin to show a gradual increase in surface roughness. The regions of increased surface roughness are referred to as mist and hackle. These regions on surface roughness are sometimes followed by crack bifurcation or branching. A microscopic examination of the fracture surface in the region of mist and hackle show that the observed roughness is a result of microscopic deviations of local sections of the crack away from the principal fracture plane.

As the surface goes from mist to hackle, the excursions become larger and proceed further from the principal fracture plane. At the point of crack branching, one of the deviations becomes large enough to nucleate a second crack which begins to propagate in a stable fashion. Several hypothesis have been put forth to explain the formation of the instability that generates the mist, hackle, and branching (Ref 24–26); however, no clear or definitive theories have yet emerged. In a qualitative sense, the formation of the instability is clearly associated with high crack velocity which accompanies a higher stress intensity. It has been suggested that either the increased velocity or the increased strain energy at the crack tip will produce the instability responsible for these FSM.

Figure 7(a) shows a schematic indicating the fracture mirror, mist, hackle, and branching pattern on a fracture surface. Figure 7(b) shows a photomicrograph of a representative fracture mirror in glass. The distance from the center of the fracture origin to the onset of mist is referred to as the mirror radius. It has been shown in several studies (Ref 27, 28) that an empirical relation of the form:

$$\sigma_f\sqrt{R_i} = A_i \qquad \text{(Eq 5)}$$

can be used to relate the mirror radius to mist, hackle, and branching to the magnitude of stress at failure ($\sigma_f$). In each case, $R$ indicates the mirror radius and $A$ is the empirically derived constant. $A_M$, $A_H$, and $A_B$ correspond to the mirror constants for mist, hackle, and branching, respectively. Mecholsky (Ref 29) has examined the fracture mirror relationship for glass failures spanning nearly two orders of magnitude in failure stress. His results (Fig 8) indicate that a single mirror constant can be applied to the entire range of failure stresses.

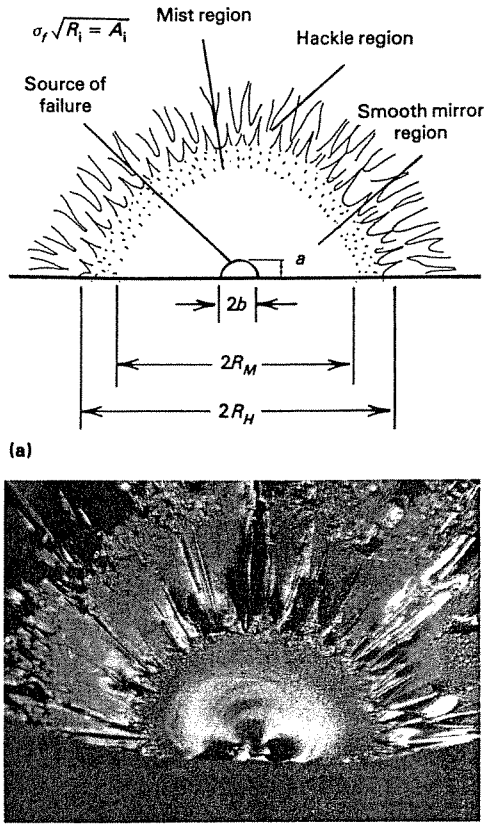


**Fig 7** (a) Schematic representation of a fracture surface showing the formation of mist and hackle that define the mirror radius. (b) Photomicrograph of fracture surface in glass showing mirror, mist, hackle, and crack branching radii. Reflected light, 10×

Equation 5 is a very important relationship in quantitative fractography, because it can be used to estimate the failure stress with good precision over a wide range of applied stresses simply by measuring the mirror radius on a failed component. An important advantage of the mirror radius method for estimating the failure stress over the use of the origin flaw size is that the mirror radius examines a portion of the fracture event where the crack has developed its equilibrium shape and is well aligned with the applied stress field. This removes some of the sources of error previously discussed in using the origin crack which may be highly complex in shape and poorly aligned with the applied stress at failure.

In many cases, the origin flaw will not be centered within the mirror boundary. This is often associated with complex flaws where the catastrophic crack preferentially nucleates from one portion of the flaw boundary. Since the mirror boundary is associated with a well-developed crack, the actual location of the origin flaw is unimportant and one should measure the complete mirror diameter and divide by two to obtain the radius.

**In determining the failure stress from a mirror radius measurement,** there are several important points which must be considered:

- The measurement technique
- The nature and uniformity of the stress field
- The presence of residual stresses

Measurement technique is important because the onset of gradual roughening associated with mist or hackle will be a subjective determination. That is, when viewed with a low-magnification stereoscopic microscope, the onset of mist or hackle may not be perceived at the same point as viewed with a high-powered optical microscope or a scanning electron microscope. For this reason, it is important to use the same observation technique during failure analysis as was used to produce the empirical mirror radius relation. It is also advisable to avoid measuring the mirror boundary along a free surface of the glass because surface damage can influence the nucleation of the mist and hackle feature

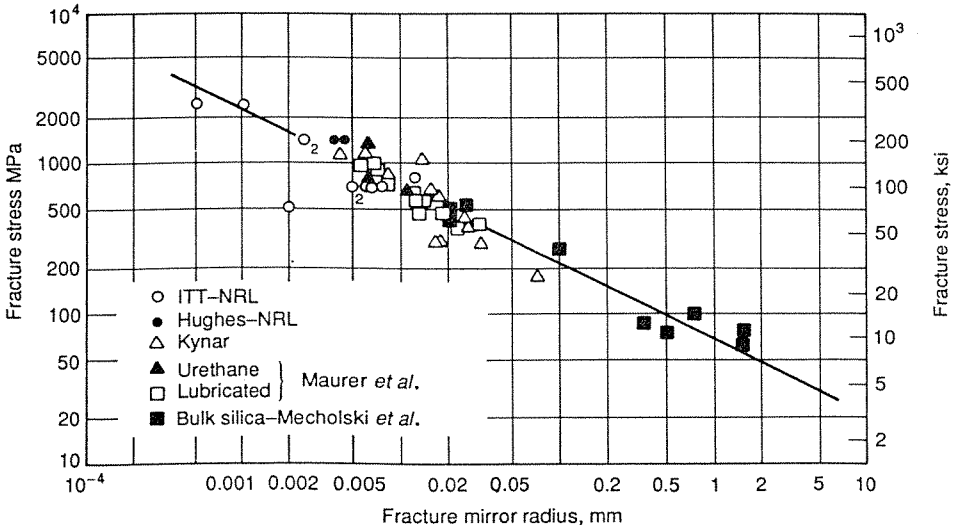


**Fig 8** Mirror radius relation obtained for silica glass fracture. Mirror radius measurements made to mist boundary. Source: Ref 29

and may result in greater uncertainties in the estimate of failure stress (Ref 27).

Another important consideration in applying the mirror radius method for failure stress is the nature of the stress field both in the empirical calibration and in the actual failure event. Figure 9, for example, shows the mirror shape obtained in bending stress condition. In bending, the applied tensile stress is maximum at one surface and decreases linearly through the thickness of the sample, reaching zero stress at the centerline and producing an equal compressive stress on the opposite surface. Obviously, a flaw spreading under the influence of this nonuniform stress field will accelerate more rapidly in the regions of high tensile stress. In Fig 9, it is clear that the fracture mirror is not uniform throughout the thickness of the sample but is generally elongated in the direction of decreasing bending stress. It is obvious that a measurement of the mirror radius in such a case will be highly dependent upon the portion of the mirror boundary that is examined. For this reason, the results of a calibration obtained in a uniform stress field may be misleading if used to estimate the failure stress for a sample that fractured in bending. However, if the mirror region in the bending failure is small with respect to the specimen dimensions (<10% of the thickness), one may consider the stress field as a uniform tensile condition and therefore obtain results that are comparable to a uniform applied tensile stress.

Little work has been done to examine the mirror radius relation for more complex, multidimensional stress fields. Mecholsky and Rice (Ref 30) have examined the fracture surfaces of a glass ceramic and a glass specimen tested in biaxial flexure. Their results indicate that the mirror radius relation describing biaxial flexure and uniaxial flexure are indistinguishable. This is very important since it may not always be possible to determine the exact nature of the stress field involved in a field failure.

Residual stresses can also have an important effect on the formation of the mirror radius. Following from previous discussion, a residual tensile stress will add to the applied stress field and increase the rate of crack propagation. The effect of this will be to accelerate the development of mist, hackle, and branching. Alternatively, a residual compressive stress can be expected to suppress the formation of the mist, hackle, and branching features. Work by Kerper and Scuderi (Ref 31) has shown that residual stresses introduced by tempering can effectively shift the mirror radius relation if the residual stresses are uniform over the region of the mirror. If the residual stresses vary over the region of the mirror, the mirror shape can be distorted, making quantitative estimates of the residual stress and applied stress difficult or impossible by post-failure radius measurements.

**The application of the mirror radius/failure stress relation to polycrystalline materials** is subject to one major limitation. The microstructure of the material can i an instability in the plane of crack pro tion that also creates fracture surface r ness. This inherent surface roughness can the features associated with mist and ha Wu *et al.* (Ref 32) has used x-ray mic diography to examine the crack path in ious polycrystalline materials and has sh that crack path instabilities that result the polycrystalline microstructure appe microbranching of the primary crack an similar to the character of mist and ha features observed on an amorphous mate The increased "background" surface ro ness can make it difficult to determine precise onset of the crack plane instabil associated with mist and hackle in polyc talline materials. In a practical sense, limitation means that the mist and hackle tures must be coarser on a polycrystal material before they can be distinguished extremely coarse-grained materials, where scale of the microstructure is on the orde the mirror size it may be impossible to id tify the mirror radius.

In cases where the microstructure eleme are much smaller than the mirror radius, mirror radius relation may be used to eva ate the stress at failure. Figure 10 shows t

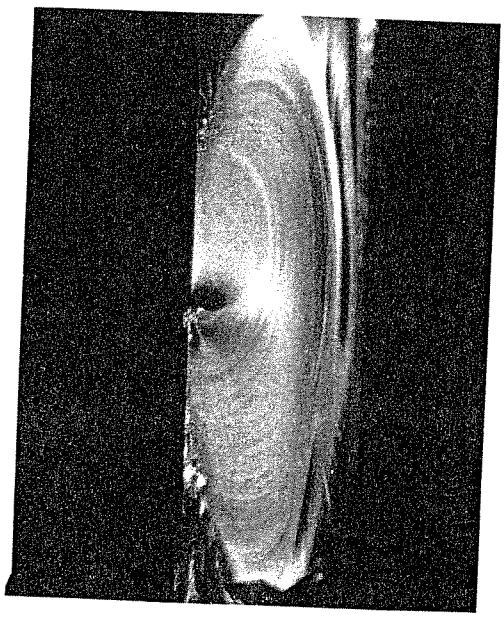

**Fig 9** Fracture mirror in glass specimen exposed to bending stress. The asymmetric mirror shape is a result of a nonuniform stress field developed in bending. Reflected light, 14×

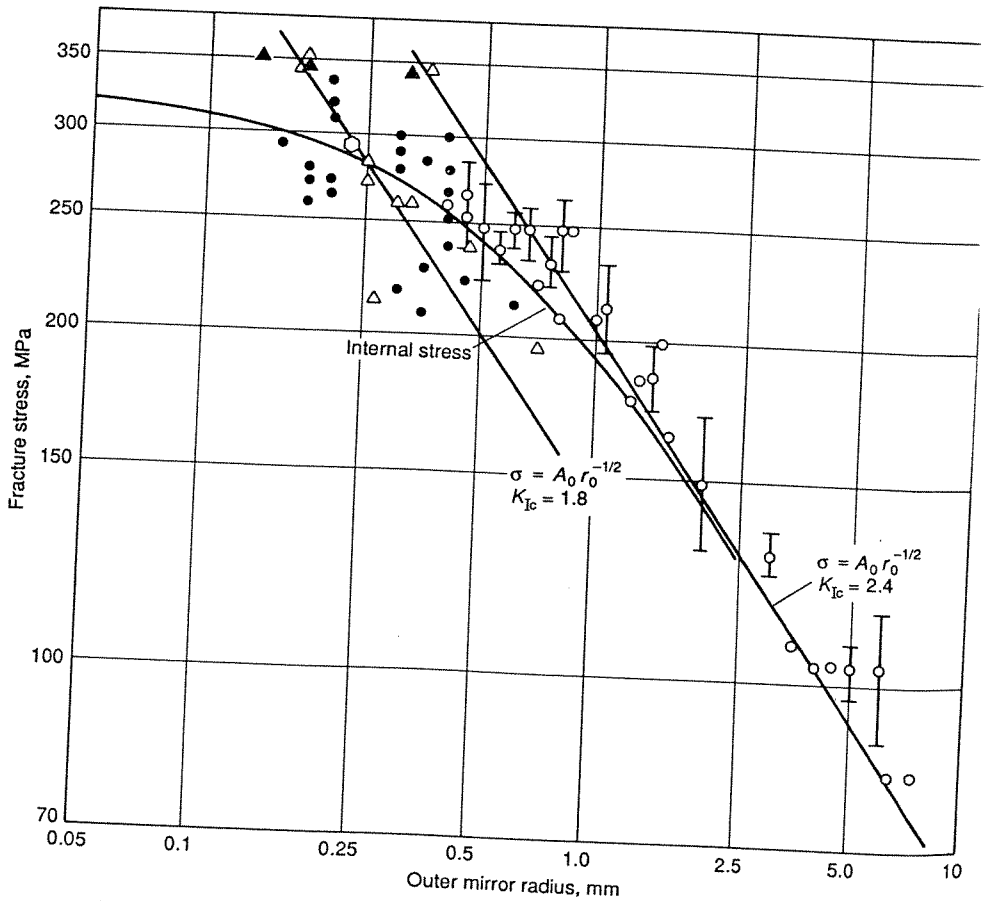


**Fig 10** Mirror radius relation determined for polycrystalline glass ceramic. Internal stresses resulting from crystal anisotropy affect mirror radius relation at small mirror dimensions. Source: Ref 34

mirror radius relation determined for a polycrystalline glass ceramic material by Rice *et al.* (Ref 33). This work shows that the expected mirror relation (Eq 5) is observed for larger mirror radius conditions. However, at smaller mirror radius (larger failure stresses) the data indicate significant deviation from the strength/mirror radius relationship. Lewis (Ref 34) has attributed this behavior to the effects of microstructural stresses that result from anisotropic thermal expansion in the individual grains of polycrystalline material. These data indicate that caution must be applied when the mirror size is on the order of the scale of the microstructure.

**Single-Crystal Fracture.** The strength/mirror radius relation has been studied to a lesser extent for the case of single-crystal fracture. The limited results indicate that the extreme anisotropy in single crystals leads to fracture mirrors that are very complex and difficult to interpret. Rice (Ref 1) has recently reviewed the work done on the fracture mirrors in single-crystal ceramic materials and gives a very comprehensive account of the state of understanding in this area. His survey suggests that the complexity in the observed fracture mirror boundaries gives more clues toward the fundamental mechanisms of mist and hackle formation rather than providing a reliable approach to quantitative estimates for failure stress.

## Crack Branching

As the developing crack continues to accelerate under the influence of the applied stress, it may branch and form multiple, stable primary fractures. The phenomenon of crack branching is a result of the same instability that generates mist and hackle on the fracture surface, and a relation similar to the mirror radius relation established in the previous section can be used to estimate the failure stress from measurements of branching radius. In this section, however, two other quantitative fractographic relations that utilize measurements of crack branching are discussed. In one case, the total number of branches that form the fragmentation pattern

**Table 1 Fragmentation patterns in thin walled structures**

| Specimen | Stress condition | Ratio of principal stresses, $\sigma_y/\sigma_x$ | Maximum angle of branching, degrees |
|---|---|---|---|
| Tube | Torsion | −1 | 15 |
| Lath | Crossbending | 0 | 45 |
| Container | Pressure | 1/2 | 90 |
| Sheet | Central pressure | 1 | 180 |

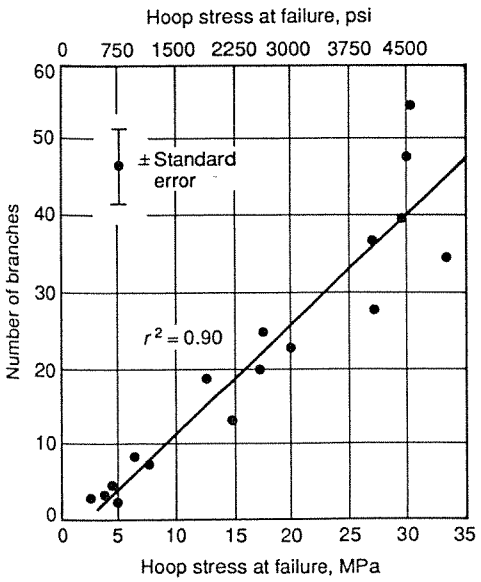


**Fig 11** Failure stress versus the number of crack branching events observed for glass containers fractured under internal pressure. Source: After Ref 35

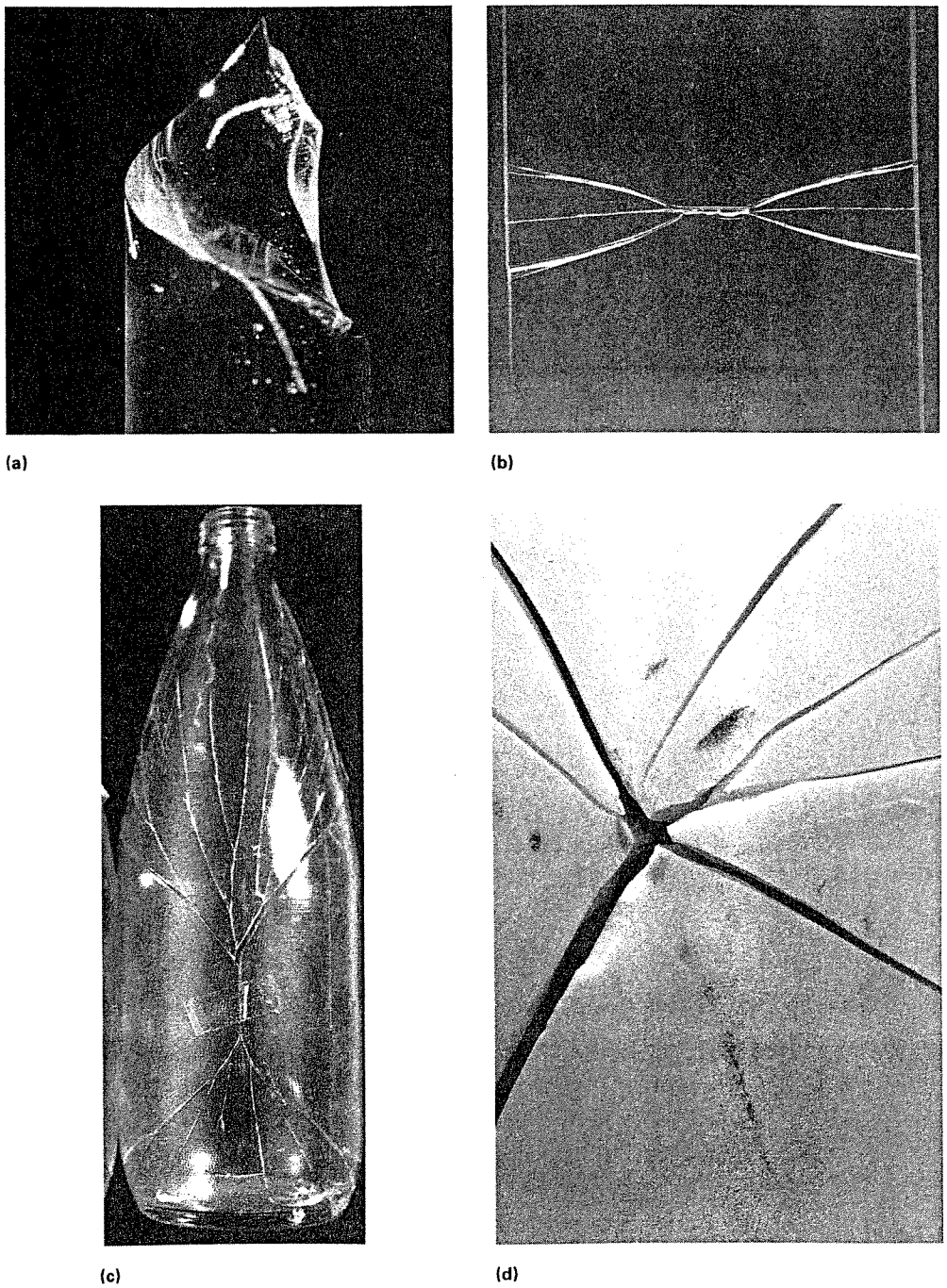


**Fig 12** Fragmentation patterns observed under various stressing conditions. (a) Torsion. (b) Crossbending. (c) Internal pressure. (d) Drumhead tension

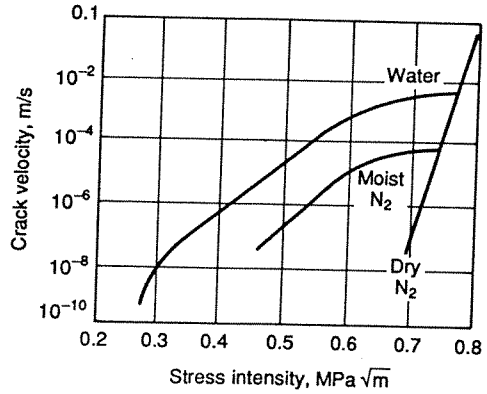


**Fig 13** Schematic representation of crack velocity versus stress intensity relation for silicate glass in moist and dry conditions

can be used to estimate the stress at failure. In another quantitative fractographic technique, crack branching geometries are used to assess the nature (uniaxial, flexure, torsion) of the stress field that was acting at the time of failure.

**Determination of Stress at Failure from Branching Patterns.** At high enough crack tip stress intensity and resultant crack velocity, a single primary crack can branch into two stable propagating cracks. If there is enough stored energy in the system, each of the new cracks can also accelerate and experience the same instability that resulted in branching of the primary crack. In this way branched cracks can themselves branch, and this process can repeat as long as there is sufficient energy to continue driving the crack acceleration process. The process of multiple crack branching results in a fragment pattern that can be used to determine magnitude of the stress at failure.

Frechette and Michalske (Ref 35) stu the fragmentation patterns for glass tainers that had failed by internal pressu tion. In these experiments, the internal pres at failure was measured and used to d mine the hoop stress at failure in the g container walls. Fractographic measurem of the mirror radius dimensions (to the and hackle boundaries) were correlated the failure stress and were found to obey empirical mirror radius/failure stress rela (Eq 5). In these experiments the fragme tion pattern was also examined, and the number of branching events was correla with the hoop stress at failure. The res given in Fig 11 show that a linear relations between the number of branching events the failure stress was discovered in th experiments. Although no models were p sented to explain the existence of this emp ical relation, a comparison of the scatter the mirror radius data with the observed sc ter in the fragmentation results indicated t the crack branching relation provided a bet method for estimating the failure stresses pressurized glass containers. It was reason that the smaller amount of scatter in t observed fragmentation relation could attributed to the averaging process inherent multiple crack branching events. That multiple crack branching samples a large po tion of the glass container and may provi a better average of the overall thickness va ations and other irregularities associated wi glass beverage containers. Alternatively, t mirror radius measurement samples a sma segment of the container and is therefore se sitive to the local distribution of geometri irregularities.

**Estimating the Ratio of Principc Stresses at Failure.** The fragmentation pa tern generated by crack branching not onl provides a means of estimating the magnitud of the applied stress at failure but can also b used to evaluate the ratio of the principa stresses acting at failure. Preston (Ref 36 shows that the included angle of branchin observed in the fragmentation pattern fits a empirical relationship (Table 1). Here th included angle represents the entire branching pattern in the case of multiple branching failures. Figure 12 shows the fragmentation patterns observed for each of the four principal stress ratios considered by Preston. Although this is only a rough relation, it can be used to interpret fractographic observations to distinguish between the most commonly observed stressing conditions responsible for failure in glass and ceramic materials.

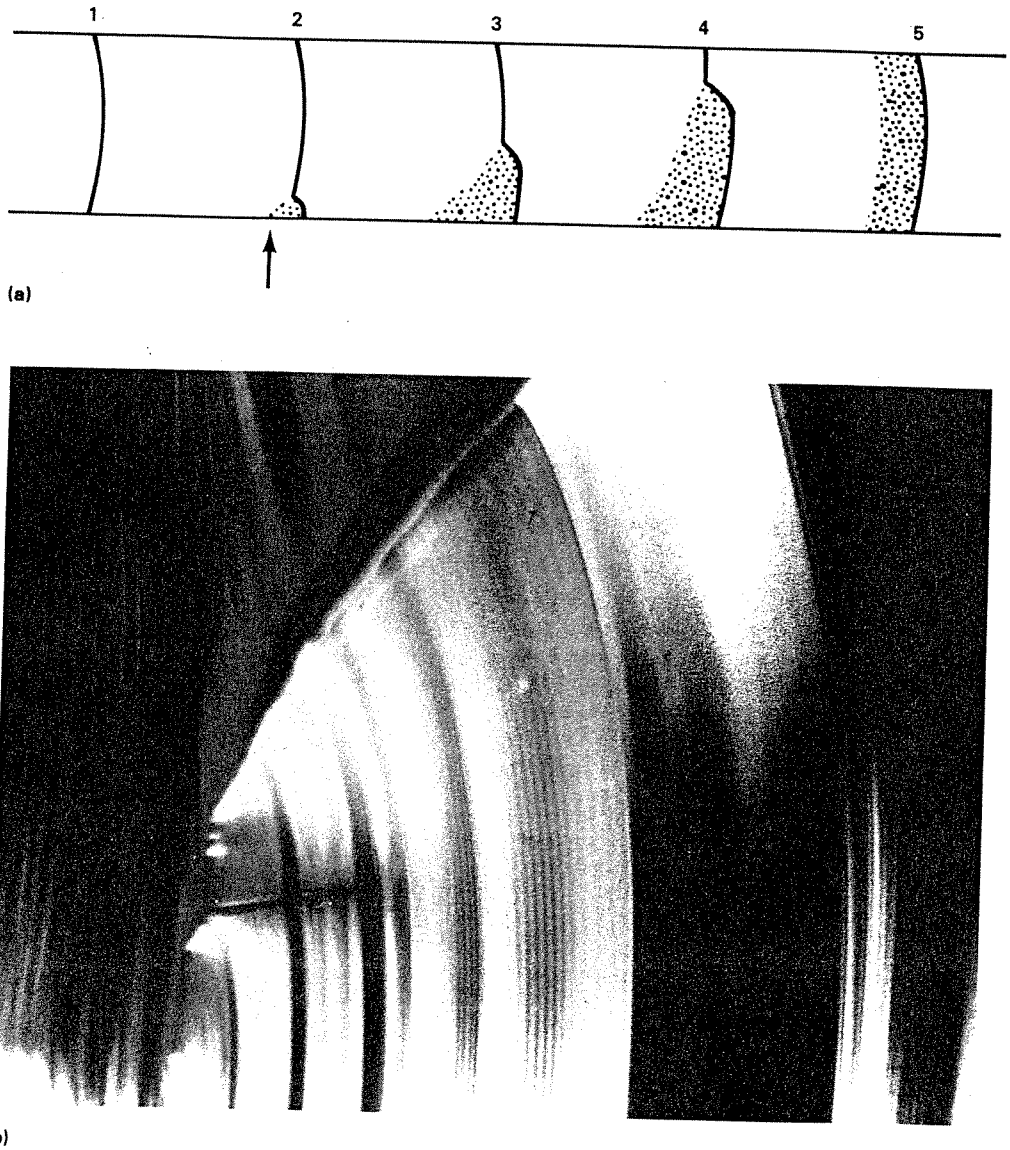


**Fig 14** (a) Stages (1 to 5 described in text) in fracture front development from a dry starter crack in a partly wetted specimen. Stippled areas indicate liquid water trailing the crack front. Arrow shows initial area of water contact. (b) Fracture surface showing intersection scarp developed at water boundary. Reflected light, 25×. Source: Ref 38

## Stress-Corrosion Fracture

It has long been recognized that glass and other ceramic materials crack more easily in

the presence of water. In fact, glaziers often apply water to the shallow crack produced by their scribing tool. The water decreases the stress required to propagate the initial crack and causes failure at a lower applied stress. The effect of water is especially pronounced for cracks that are growing very slowly (<1 cm/s). Figure 13 shows a $K_I$ versus $V$ plot for silicate glass indicating that the presence of water as a liquid or gas enhances the rate of crack propagation in the low stress intensity regime.

The extremely slow growth of a surface crack is very important because it can give rise to a phenomenon know as delayed failure. Delayed failure causes structures that have supported a load for long periods of time to suddenly and spontaneously fail. Longer flaws concentrate more stress and can result in catastrophic failure at smaller applied stresses. In the case of delayed failure, a small flaw can grow under the influence of the applied stress and water in the surrounding environment until it is large enough to cause catastrophic failure. Previous studies have shown that long-term failure stress may be as small as one-fourth the measured short-term (rapid) failure strength.

Because water can have such a profound effect on the strength and mechanical durability of glass and ceramic materials, it is often important to determine whether stress-corrosion fracture was responsible for a specific field failure. This section describes indirect and direct fractographic techniques that can be used to identify the presence of water during the fracture event. An indirect method for determining the stress-corrosion conditions involves the use of the mirror-to-flaw size ratio. It has also been shown that the presence of liquid water in the propagating crack will also produce unique FSM that can be used to directly assess the nature of the stress-corrosion conditions.

**Indirect fractographic evidence of water in field failures** utilizes fracture surface markings to assess the extent of slow crack growth that preceded the catastrophic failure event. In stress-corrosion assisted delayed failure, the initial flaw will slowly extend until the stress intensity (see Eq 2) reaches a critical value where catastrophic failure can occur. This means that a failure stress estimated from the initial flaw size (see the section "Origin Flaw") will overestimate the actual failure stress. In field failure, the actual magnitude of the failure stress is more than likely not known. However, the failure stress can be accurately estimated by measuring the mirror radius to mist or hackle. (During catastrophic failure event, the development of mist and hackle will be independent of the water in the surrounding environment because the crack will be moving too fast for the water to keep up with the moving crack. Therefore, the mirror radius only represents the stress level at failure according to the mirror relationship shown in Eq 5.) Using the mirror size to scale the level of applied stress, one finds that the ratio of the mirror radius to the initial flaw size will be larger for the case of stress-corrosion fracture than for the case where no environmental effects influence the failure process.

Mecholsky (Ref 37) has examined the mirror-to-flaw-size ratio for glass and ceramic specimens that failed under long-term static loading. In an example of a silicate glass specimen that failed after 200 hours under load, a mirror-to-flaw-size ratio of 80 was observed. The same glass tested in rapid loading conditions (no stress-corrosion effects) gave a mirror-to-flaw-size ratio of 13. This and other results reported by Mecholsky (Ref 37) for the failure of polycrystalline ceramic materials such as $MgF_2$ indicate that the presence of stress-corrosion failure can be evaluated by a post-failure examination of the fracture surfaces. In addition, the authors present a fracture mechanics analysis that can be used to relate the mirror-to-flaw-size ratio to the total time under load for the delayed failure event and found good correlation between the times predicted by this fractographic and the experimentally measured failure times.

Although this indirect fractographic method represents an important technique for identifying stress-corrosion failure conditions, its usefulness depends strongly upon ones ability to accurately measure the size of the initial flaw. As is discussed in the section "Origin Flaw," measurements of the initial flaw size are subject to the complexity of the surface flaw and its alignment with the direction of the applied stress field. The same cautions outlined in the discussion of origin flaws must also apply to the assessment of the mirror-to-flaw-size ratio measurements.

**Intersection Scarp.** In addition to indirect fractographic evidence for stress-corrosion failure, there are FSM that result directly from

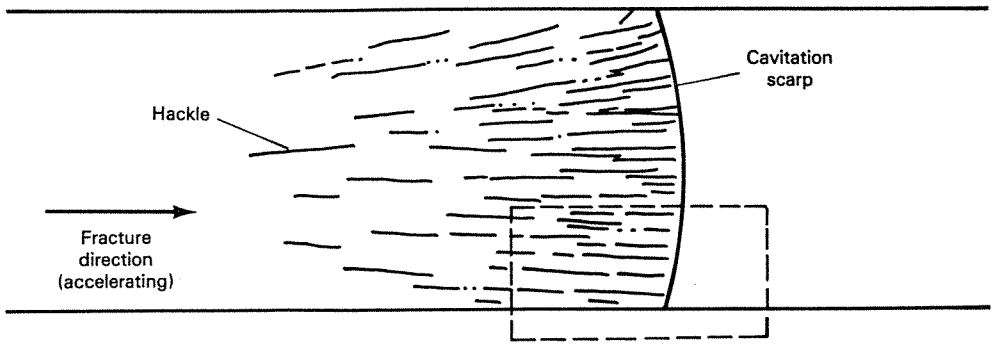


(a)

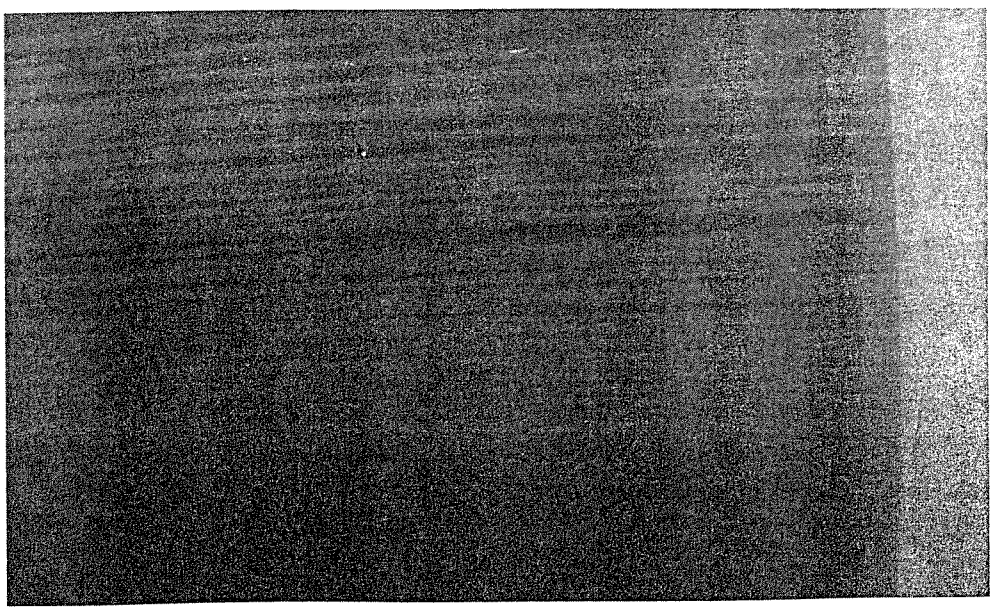

(b)

**Fig 15** (a) Schematic of exposed surface of glass fracture accelerated in water. With increasing velocity, initially mirror-smooth surface (far left) shows generation of hackle steps, followed by a cavitation scarp and the return to mirror-smooth condition at greater velocity. (b) Micrograph of area within dashed lines of schematic. Differential interference contrast, 100×. Source: Ref 39

the presence of liquid water in the propagating crack. The first of these features is called an intersection scarp (Ref 38).

Intersection scarp is formed at the boundary between wet and dry portions of a crack front which is propagating in an environment with limited access to water. Specifically, crack fronts that are partly wetted by a source of liquid water are found to develop fracture surface markings at the boundary between wet and dry areas on the crack front. The fracture surface markings developed in this way are also called intersection scarps because they are ridges (scarps) that form at the intersection of the wet and dry portions along the crack front.

Figure 14(a) shows the sequence of events that is observed as a dry crack (free of liquid), propagating a glass plate, encounters water on the specimen surface. At position 1, the normal through thickness crack front shape is observed. At position 2, the propagating crack front encounters liquid water on the free surface of the glass plate. At this time, two events take place: capillary action draws some water into contact with the moving crack front, and the wetted portion of the crack front jogs slightly ahead of the dry section. Positions 4 and 5 represent the continued spread of water across the moving crack front. At position 5, the crack is completely wet and the normal crack front shape is reformed. Figure 14(b) is a photomicrograph showing a fracture surface in a soda-lime silica glass prepared in a manner previously described.

Formation of the intersection scarp can be interpreted on the basis of the $K_I$ versus $V$ diagram (Fig 13). At velocities below 0.2 mm/s (8 mil/s), the wetted portion of the crack front propagates more easily than the dry. (In this case, dry refers to the portion of the crack front exposed to room air.) Accordingly, the wet section requires less stress to propagate and is slightly ahead of the dry section. (The magnitude of this displacement is limited because the advance of one section will increase the mechanical loading on the other.) Because the conditions of fracture are different on the wet and dry portions of the crack front, the individual planes of fracture also differ. This difference in crack plane results in a sharp ridge or scarp at the line of intersection.

The intersection shows that water was present at the time of failure. This information would be of interest in a forensic case where it may be important to know if it was raining at the time of an incident or in questions of thermal shock fracture when the exact nature of the thermal shock event is unknown.

**Cavitation Scarp.** Another form of scarp marking is developed when liquid in a crack cavitates. Michalske *et al.* (Ref 39) examined the fracture surface markings that are generated as a crack is accelerated to catastrophic velocities (>1 mm/s) in a liquid environment. Figure 15(a) is a schematic of the fracture surface markings generated when an edge cracked plate specimen accelerates in liquid water. At low velocity (left side of sketch), the crack surface appears mirror-smooth. As the velocity increases to approximately 10 mm/s (0.4 in./s), fine hackle ridges running parallel to the direction of fracture are observed on the fracture exposed surface, terminated by a distinct change in plane of the fracture surface. The fracture surface marking representing this change in plane is termed a cavitation scarp. After cavitation scarp formation, the fracture surface returns to a mirror-smooth condition. Figure 15(b) is a photomicrograph of the fracture surface of a soda-lime silica glass plate showing these features.

The process of liquid cavitation in the moving crack was modeled by Michalske and Frechette (Ref 39) by determining the negative pressure on the liquid due to viscous effects. The calculated velocity for cavit to occur was found to be in excellent ag ment with the measured velocity of cavit scarp formation for a number of different uids tested. Because cavitation scarp re from the liquid cavitation phenomena, it m the end of environment-affected, stress- rosion crack growth.

**Example 1: Interpretation of FSM a a Transition from Slow to Rapid Fract in a Liquid Environment.** Because dynamic effects of liquids involve visc drag effects, it is important to examine l those effects may operate in different cr geometries. Surface flaw geometry is greatest practical importance since surf flaws are the most common strength-cont ling defects in glass. Figure 16(a) is a sc matic showing the fracture surface marki

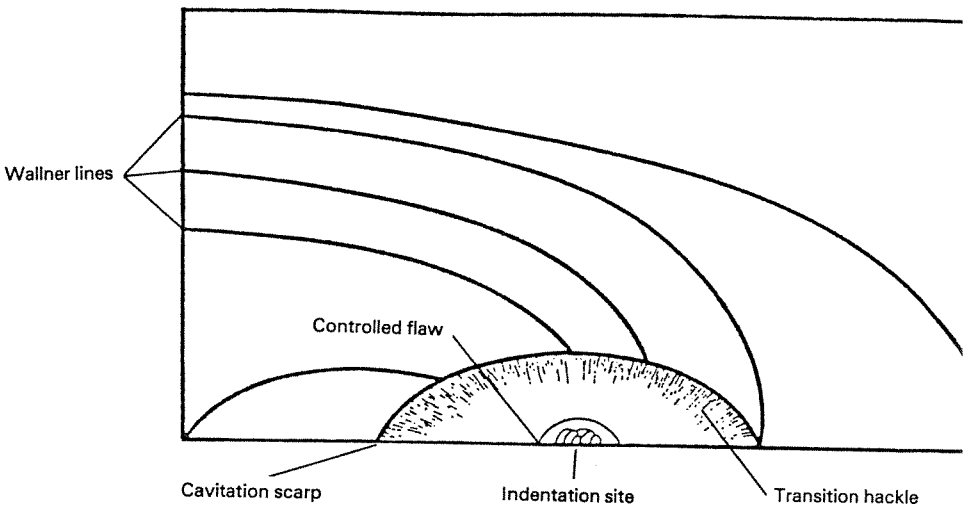


(a)

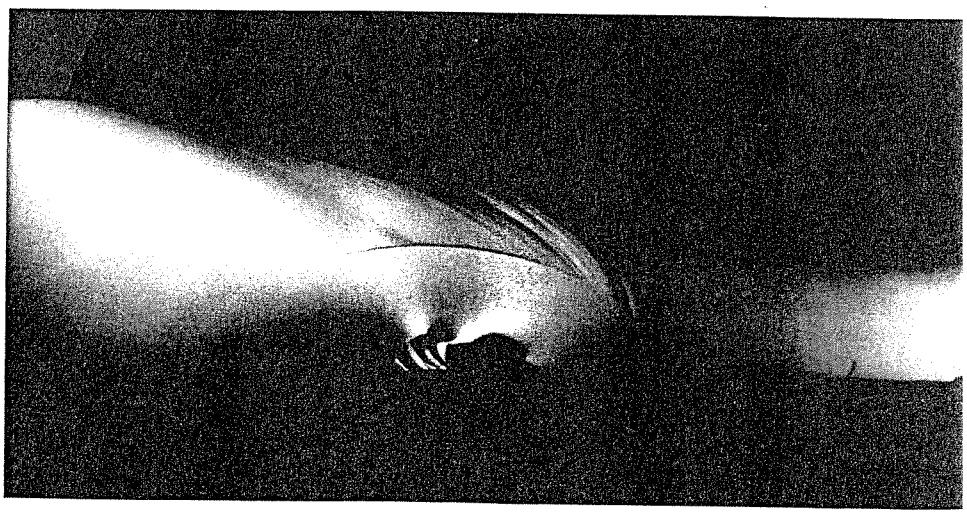

(b)

**Fig 16** (a) Schematic of exposed surface of glass fracture resulting from bending in water. (b) Microgr showing fracture surface represented in schematic. Reflected light, 15×. Source: Ref 40

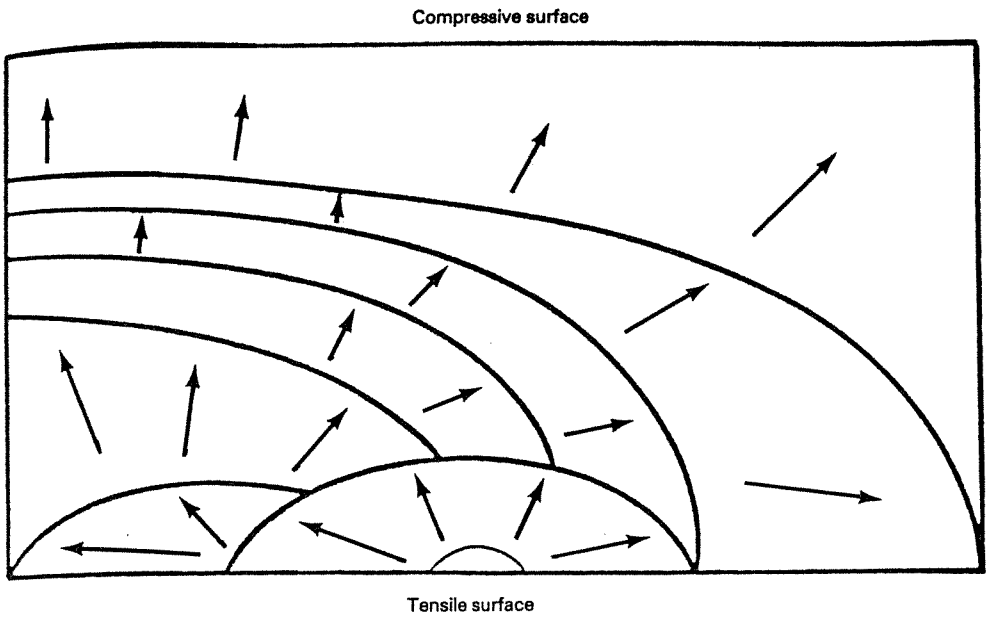


**Fig 17** Schematic showing the development of a surface flaw by application of bending stresses in water. Arrows indicate direction of local fracture.

observed when a surface flaw in soda-lime-silica glass is accelerated to critical velocity in a liquid water environment (Ref 40). The indentation flaw was used to serve as the origin of failure in this experiment and was present in the surface before the external stresses were applied. As external stress was applied to the sample, the fracture spread out into the thickness of the sample and a region of mirror-smooth surface was generated surrounding the origin flaw. Next, fine hackle ridges termed "transition hackle" developed as the origin crack accelerated under the applied stress. The transition hackle that developed in the surface flaw case was found to be identical to that observed on the edge cracked specimen. The surface flaw specimen also shows formation of a cavitation scarp which sharply terminates the transition hackle. Subsequent to the cavitation scarp are a series of Wallner lines indicating the growth pattern during the rapid fracture regime. Figure 16(b) is a photomicrograph of a soda-lime silica glass bar broken in such a manner.

In Fig 17, the arrows show the crack growth pattern that was deduced from the fracture surface markings. Initially, the origin flaw grows in all directions, spreading more rapidly along the tensile surface to form a semi-elliptical front. Following the cavitation scarp, the crack spreads preferentially from the left side of the ellipse formed by the cavitation scarp, sweeping in all directions to cause complete failure of the specimen. The fact that the crack spread preferentially (instead of evenly) from one side of the cavitation scarp is attributed to the effects of viscous drag. Along the tensile surface of the bend specimen, where the stress is highest, the crack velocity is also greatest. The gradient in stress associated with the bending geometry is responsible for the elliptical shape of the growing surface crack.

Because the crack accelerates faster along the tensile surface, the velocity required for cavitation occurs first at the surface so that one end of the ellipse will serve as the site for cavitation. After cavitation has occurred on one portion of the crack front, the increased rate of crack propagation (~10-fold) allows that portion of the crack to sweep around, intersecting those portions still wet and subject to the effects of viscous drag. (The remaining wet section of the crack is unable to cavitate because its velocity is too low.) Therefore, the majority of the crack spreading from the origin flaw is retarded by the viscous drag of the liquid phase and remains "stationary," while the water-free section rapidly advances to catastrophic velocity.

This interpretation has several important implications. First, it provides an understanding of the mechanism responsible for the transition from slow to rapid fracture in liquid environments. Wiederhorn (Ref 41) has shown that this information is essential to the models used to predict the effect of proof testing on the strength. The cavitation scarp is also important in its role of defining the size of the flaw present at the onset of catastrophic failure. The critical flaw size is necessary to the calculation of the $K_{Ic}$ value measured in a stress-corrosion environment. It is important to note here that critical flaw size as taken from the cavitation scarp must be measured from the center of the origin flaw to the point on the scarp where cavitation initiated. Finally, after the $K_{Ic}$ has been measured by this technique, the stress at failure may be calculated (using Eq 2) from a post-failure measurement on the failed component.

## REFERENCES


1. R.W. Rice, Perspective on Fractography, *Advances in Ceramics,* Vol 22, *Fractography of Glasses and Ceramics,* J.R. Varner and V.D. Frechette, Ed., The American Ceramic Society, 1988, p 3–56
2. V.D. Frechette, The Fractography of Glass, *Introduction to Glass Science,* L.D. Pye, H.J. Stevens, and W.C. LaCourse, Ed., Plenum Press, 1972, p 433–450
3. R.W. Rice, Ceramic Fracture Features, Observations, Mechanisms, and Uses, *Fractography of Ceramic and Metal Failures,* J.J. Mecholsky and S.R. Powell, Ed., American Society for Testing and Materials, 1984, p 5–102
4. S.W. Freiman, A Critical Evaluation of Fracture Mechanics Techniques for Brittle Materials, *Fracture Mechanics of Ceramics,* Vol 6, R.C. Bradt, A.G. Evans, D.P.A. Hassleman, and F.F. Lange, Ed., Plenum Press, 1983, p 27–45
5. *The Ceramic Source,* Vol 6, The American Ceramic Society, 1991
6. S.W. Freiman, T.L. Baker, and J.B. Wachtman, "A Computerized Fracture Mechanics Database for Oxide Glasses," Technical Note 1212, National Bureau of Standards, 1985
7. H. Tada, P. Paris, and G. Irwin, *The Stress Analysis of Cracks Handbook,* Del Research Corporation, 1973
8. J.J. Mecholsky and S.W. Freiman, Determination of Fracture Mechanics Parameters Through Fractographic Analysis of Ceramics, *STP 678,* American Society for Testing and Materials, 1980, p 136–150
9. R.W. Rice, S.W. Freiman, and P.F. Becher, Grain-Size Dependence of Fracture Energy in Ceramics: I, Experiment, *J. Am. Ceram. Soc.,* Vol 64 (No. 6), 1981, p 345–350
10. P.L. Swanson, Crack-Interface Traction: A Fracture-Resistance Mechanism in Brittle Polycrystals, *Advances in Ceramics,* Vol 22, *Fractography of Glasses and Ceramics,* J.R. Varner and V.D. Frechette, Ed., The American Ceramic Society, 1988, p 135–155
11. J.W. Dally and W.F. Riley, *Experimental Stress Analysis,* McGraw-Hill, 1965
12. H. Hertz, *Hertz's Miscellaneous Papers,* MacMillan, London, 1986
13. B.R. Lawn, S.M. Wiederhorn, and H.H. Johnson, Strength Degradation of Brittle Surfaces: Blunt Indenters, *J. Am. Ceram. Soc.,* Vol 58 (No. 9–10), 1975, p 428–432
14. D.B. Marshall and B.R. Lawn, *J. Mater. Sci.,* Vol 14, 1979, p 2001–2012

15. A.W. Ruff and S.M. Wiederhorn, Erosion by Solid Particle Impact, *Treatise on Plat. Sci. and Tech.*, Vol 16, C.M. Preece, Ed., Academic Press, 1979, p 69–126
16. V.H. Wallner, Linienstrukturen an Bruchflachen 2, *Phys.*, Vol 114, 1939, p 368–378
17. E.F. Poncelet, The Markings on Fracture Surfaces, *J. Soc. Glass Technol.*, Vol 42, 1958, p 279T
18. F. Kerhof, *Naturwissenschaften*, Vol 40, 1953, p 478
19. F. Kerhof, *Kurzzeitphysik*, K. Vollrath and G. Thomer, Ed., Springer-Verlag, 1967, p 498
20. F. Kerhof and H. Dreizler, *Glastechnische Berichte*, Vol 29 (1956), p 459
21. T.A. Michalske and V.D. Frechette, Modified Sonic Technique for Crack Velocity Measurement, *Int. J. Fracture*, Vol 17 (No. 3), 1981, p 251–256
22. T.A. Michalske, M. Singh, and V.D. Frechette, Experimental Observation of Crack Velocity and Crack Front Shape Effects in Double-Torsion Fracture Mechanics Tests, *Fracture Mechanics of Ceramics Rocks and Concrete*, E.R. Fuller and S.W. Freiman, Ed., American Society for Testing and Materials, 1981, p 3–12
23. T.A. Michalske and J.M. Collins, Fractographic Determination of Crack Tip Stress Intensity, *Advances in Ceramics*, Vol 22, *Fractography of Glasses and Ceramics*, J.R. Varner and V.D. Frechette, Ed., The American Ceramic Society, 1988, p 229–239
24. E.H. Joffe, The Moving Griffith Crack, *Philos. Mag.*, Vol 42 (No. 112), 1951, p 739–750
25. W. Doell, Investigations of Crack Branching Energy, *Int. J. Fracture*, Vol 11, 1975, p 184–186
26. H.P. Kirchner and J.W. Kirchner, Fracture Mechanics of Fracture Mirrors, *J. Am. Ceram. Soc.*, Vol 62 (No. 3–4), 1979, p 198–202
27. E.B. Shand, Breaking Stress of Glass as Determined from Dimensions of Fracture Mirrors, *J. Am. Ceram. Soc.*, Vol 42 (No. 10), 1959, p 474–477
28. N. Terao, Relation Between Resistance to Rupture and Mirror Surface in Glass, *J. Phys. Soc. Jpn.*, Vol 8, 1953, p 545–549
29. J.J. Mecholsky, S.W. Freiman, and S.M. Morey, Fracture Surface Analysis of Optical Fibers, *Fiber Optics: Advances in Research and Development*, B. Bendow and S.S. Mitra, Ed., Plenum, 1979, p 187–208
30. J.J. Mecholsky, Jr. and R.W. Rice, Fractographic Analysis of Biaxial Failure in Ceramics, *Fractography of Ceramic and Metal Failures*, ASTM STP 827, J.J. Mecholsky, Jr. and S.R. Powell, Jr., Ed., American Society for Testing and Materials, 1984, p 185–193
31. M.J. Kerper and T.G. Scuderi, Modulus of Rupture of Glass in Relation to Fracture Pattern, *Am. Ceram. Soc. Bull.*, Vol 44 (No. 12), 1965, p 953–955
32. C.Cm. Wu, S.W. Freiman, R.W. Rice, and J.J. Mecholsky, Microstructural Aspects of Crack Propagation in Ceramics, *J. Mater. Sci.*, Vol 13, 1978, p 2659–2670
33. R.W. Rice, R.C. Pohanka, and W.J. McDonough, Effect of Stresses from Thermal Expansion Anisotropy, Phase Transformations, and Second Phases on the Strength of Ceramics, *J. Am. C Soc.*, Vol 63 (No. 11–12), 1980, p 710
34. D. Lewis, III, Fracture Strengtl Mirror Size in a Commercial Ceramic, *J. Am. Ceram. Soc.*, V (No. 2), 1981, p 82–86
35. T.A. Michalske and V.D. Frec Fragmentation in Bursting Glass tainers, *Bull. Am. Ceram. Soc.*, V (No. 4), 1978, p 427–429
36. F.W. Preston, Angle of Forking of Cracks as an Indicator of the Stress tem, *J. Am. Ceram. Soc.*, Vol 18, p 175
37. J.J. Mecholsky and S.W. Freiman, tographic Analysis of Delayed Failu Ceramics, *Fractography and Mate Science*, ASTM STP 733, Amer Society for Testing and Materials, 1 p 246–258
38. T.A. Michalske, J.R. Varner, and Frechette, Growth of Cracks Partly F with Water, *Fracture Mechanics Ceramics*, Vol 4, R.C. Bradt, D.I Hassleman, and F.F. Lange, Plenum, 1978, p 639–649
39. T.A. Michalske and V.D. Freche Dynamic Effects of Liquids on Cr Growth in Glass, *J. Am. Ceram. S* Vol 63 (No. 11–12), 1980, p 603–6
40. T.A. Michalske, V.D. Frechette, anc Hudson, Dynamic Effects of Liquids Surface Crack Extension in Gl *Advances in Fracture Research*, Vol D. Francis, Ed., Pergamon, 1981, 1091–1097
41. E.R. Fuller, S.M. Wiederhorn, J.E. F ter, and P.B. Oates, Proof Testing Ceramics, *J. Mater. Sci.*, Vol 15, 19 p 2282–2295